The PGE_2/Ptger4b pathway regulates ovulation by inducing intracellular actin cytoskeleton rearrangement via the Rho/Rock pathway in the granulosa cells of periovulatory follicles in the teleost medaka

Katsueki Ogiwara[§], Chika Fujimori, and Takayuki Takahashi

Laboratory of Reproductive and Developmental Biology, Faculty of Science, Hokkaido University, Sapporo 060–0810, Japan

[§]Corresponding author:

Katsueki Ogiwara, Laboratory of Reproductive and Developmental Biology, Faculty of Science, Hokkaido University, Sapporo 060–0810, Japan

Tel: 81–11–706–2748

Fax: 81–11–706–4456

E-mail: kogi@sci.hokudai.ac.jp

Keywords: medaka ovulation, PGE_2, Ptger4b, Rho, Rock, intracellular actin cytoskeleton rearrangement

Abstract

We have previously shown that the prostaglandin E_2/Ptger4b receptor system is involved in ovulation in teleost medaka and induces intracellular actin cytoskeleton rearrangement in the granulosa cells of preovulatory follicles. In this study, we investigated the signaling pathways through which prostaglandin E_2 induces a change in the actin cytoskeleton. Treating preovulatory follicles with GW627368X (Ptger4b antagonist), a Rho inhibitor, or Y-27632 [Rho-associated protein kinase (Rock) inhibitor] inhibited not only in vitro follicle ovulation but also intracellular actin cytoskeleton rearrangement. Active Rhoa-c and Rock1 were detected in follicles immediately before ovulation. GW627368X also inhibited Rhoa-c activation and cytoskeleton rearrangement. PGE_2-induced actin cytoskeleton rearrangement was not observed in the Ptger4b-, Rhoa-c-, or Rock1-deficient OLHNI-2 cells. These results indicate that the PGE_2/Ptger4b pathway regulates intracellular actin cytoskeleton rearrangement via the Rho/Rock pathway in the granulosa cells of preovulatory follicles during medaka ovulation.

1. Introduction

Ovulation is a dynamic process of extrusion of mature oocytes from the interior of the ovary into the ovarian or peritoneal cavity, depending on the species (Espey and Richards, 2006; Lubzens et al., 2010), and is induced by the ovulatory surge of gonadotropin luteinizing hormone (LH). This process is closely coordinated by several intracellular and extracellular factors, proteins, and low-molecular-weight substances, including steroid hormones and prostaglandins (PGs). Previous studies have established that many genes/proteins are regulated and induced in the preovulatory follicles in response to LH stimulation, particularly in granulosa cells (GCs). These ovulation-associated genes/proteins have been studied intensively and the information from such studies aids in understanding the nature of LH-induced ovulation in vertebrates (Christenson et al., 2013; Espey and Richards, 2002; Espey and Richards, 2006; Gilbert et al., 2011; Lussier et al., 2017; Richards, 2007; Richards et al., 2015).

It is generally accepted that proteolytic degradation of the follicle wall extracellular matrix (ECM) components in the apical region of ovulating follicles is indispensable for successful vertebrate ovulation. However, the proteolytic enzymes responsible for follicle rupture have not yet been identified. In contrast, the mechanism underlying follicle wall degradation has been intensively studied in the teleost medaka. Sequential actions of two

60 distinct proteolytic enzyme systems, the urokinase-type plasminogen activator/plasmin
61 system (Ogiwara et al., 2015) and the matrix metalloproteinase (MMP) system (Ogiwara
62 et al., 2005), are required for the hydrolysis of ECM proteins present in the layers of
63 ovulating follicles. Activation/regulation by intrinsic inhibitors and the roles of individual
64 proteolytic enzymes involved in follicle rupture have been established (Takahashi et al.,
65 2019). More recently, the signaling pathway of the LH-induced expression of MMP-15
66 (also known as MT2-MMP), one of the three MMPs required for follicle rupture during
67 ovulation, has been elucidated (Ogiwara et al., 2021).

68 PGs are a group of biologically active lipid compounds that participate in various
69 physiological processes in vertebrates. PGs have been implicated as important inducers
70 of ovulation in many vertebrate species (Kim and Duffy, 2016; Richards, 1997; Sena and
71 Liu, 2008; Shimada et al., 1986; Sorensen and Goetz, 1993; Takahashi et al., 2013). Mice
72 deficient in cyclooxygenase-2, the rate-limiting enzyme in PG synthesis, exhibit an
73 anovulatory phenotype (Davis et al., 1999). In addition, ovulation rate is reduced in mice
74 lacking the PGE_2 receptor subtype EP2 (Hizaki et al., 1999, Kennedy et al., 1999, Tilley
75 et al., 1999). These findings, together with those of ablate-and-replace experiments in
76 nonhuman primates (Duffy et al., 2019), have established the role of PGE_2 and its receptor,
77 EP2, in the ovulatory process in mammals. An interesting finding from experiments using

78 EP2-knockout mice is that the cumulus-oocyte complex (COC) is abortive in multiple
79 ovulated complexes, indicating that the PGE_2/EP2 receptor system activated after LH
80 stimulation also plays a role in COC expansion in periovulatory follicles (Hizaki et al.,
81 1999). However, the mechanisms underlying PGE_2-induced ovulation are not yet fully
82 understood. Accumulating evidence indicate a critical role of PGs in teleost ovulation.
83 $PGF_{2\alpha}$ and/or PGE_2 play important roles in the ovulatory processes in fish (Takahashi et
84 al., 2018). In vitro ovulation has been shown to be inhibited by indomethacin using yellow
85 perch (Bradley et al., 1994), Japanese eel (Kagawa et al., 2003), zebrafish (Lister et al.,
86 2008) and medaka (Fujimori et al., 2011). In medaka, in which PGE_2 regulates ovulation
87 (Fujimori et al., 2011; Fujimori et al., 2012), the PGE_2 receptor subtype Ptger4b is
88 drastically induced in an LH-dependent manner in large-sized follicles as ovulation
89 approaches. Similar to medaka, studies have demonstrated that Pgr and Ptger4b have
90 pivotal roles in zebrafish ovulation (Baker et al 2019; Baker and Van Der Kraak, 2021;
91 Tang et al., 2016), favoring the possibility of a functional role of PGE_2 in ovulation across
92 teleost species. Despite evidences supporting the contribution of PGE_2 to teleost ovulation,
93 the mechanism by which PGE_2 promotes ovulation remains largely unknown. However,
94 in this context, we previously reported that Ptger4b receptor activation by PGE_2 in the
95 GCs of ovulating follicles of medaka progressively leads to actin depolymerization within

96 the cells as the time of ovulation approaches (Ogiwara and Takahashi, 2016), suggesting
97 a role for the PGE_2/Ptger4b system in actin cytoskeleton remodeling in the GCs of
98 follicles at follicle rupture during ovulation.

99 Dynamic remodeling of the actin cytoskeleton involves the physiological processes,
100 such as cell migration, invasion, and metastasis (Yamaguchi and Condeelis, 2007). The
101 remodeling is regulated by actin polymerization and depolymerization. Rho GTPases,
102 such as Rac, Rho, and Cdc42, are the main regulators of remodeling and play pivotal roles
103 in controlling actin cytoskeleton dynamics (Ridley, 2001). Regulators, such as cofilin,
104 cortactin, LASP-1, Mena, AFAP-110, and profilin are also reported to be involved in
105 controlling the actin cytoskeleton (Najm and El-Sibai, 2014; Yamaguchi and Condeelis,
106 2007). Some studies suggest that the reorganization of the actin cytoskeleton is regulated
107 via the PGE_2/EP pathway in many cellular systems. Adhesion dynamics in dendritic cells
108 are mediated via the PGE_2/EP pathway (van Helden et al., 2008). It is suggested that
109 PGE_2/EP4 signaling mediates actin filament depolymerization in podocytes, resulting in
110 the suppression of filtration barrier function in the cells (Martineau et al., 2004). PGE_2/EP
111 signaling has been demonstrated to modulate the migration of dendritic cells by
112 reorganizing the F-actin cytoskeleton (Diao et al., 2021). The above studies have also
113 shown that cAMP acts as a signaling molecule downstream of the PGE_2 receptor.

To extend our hypothesis that the activated PGE_2/Ptger4b system in medaka follicles around the time of follicle rupture induces intracellular actin cytoskeleton rearrangement in follicle cells (Ogiwara and Takahashi, 2016; Takahashi et al., 2018), we examined the signaling pathway involved in the PGE_2/Ptger4b system that leads to cytoskeleton rearrangement during ovulation in medaka. Herein, we report a possible role for the Rho/Rho-associated protein kinase (Rock) pathway in actin rearrangement in the GCs of periovulatory follicles. Our results strengthen the notion that PGE_2 plays a pivotal role in intracellular actin filament rearrangement in the GCs of periovulatory follicles during ovulation in the fish.

2. Materials and methods

2.1. Medaka culture and tissue preparation

Orange-colored medaka fish (*Oryzias latipes*) variants purchased from commercial vendors were used in this study. The fish were kept in a 60-liter tank for at least 14 days to acclimate to 26 °C under a 14/10 h light/dark cycle (Ogiwara et al., 2005). Under these conditions, they spawn daily and ovulate immediately before the light period begins. In this study, the timing, called ovulation time, was set at ovulation hour 0. Preovulatory follicles destined to ovulate (≥1.0 mm, post-vitellogenic phase, stage IX-X) were isolated

(Ogiwara et al., 2013). The follicle layers were separated as previously described (Ogiwara et al., 2005). The experimental procedures used in this study were approved by the Committee of the Experimental Plants and Animals, Hokkaido University.

2.2. In vitro follicle culture and ovulation

In vitro follicle culture was performed as described previously (Ogiwara and Takahashi, 2019). Preovulatory follicles already exposed to the endogenous LH surge were isolated from the ovary 3 h before ovulation and cultured at 26 °C in 90% M199 medium (pH 7.4) with or without 10 μM GW627368X, 0.1-2.5 μg/mL Rho inhibitor (Cytoskeleton, Inc.; Denver, CO), 10 μM ML 141 (Tocris Bioscience; Ellisville, MO), 50 μM Rac1 inhibitor (Wako, Osaka, Japan), 1 μg/mL Rho activator (Cytoskeleton, Inc.), and 0.1-10 μM Y-27632 (Rock inhibitor, Wako). After culturing for 3, 4, 6, or 8 h, the follicles were collected and used for subsequent experiments. The ovulation rate was determined by counting the number of oocytes that successfully ovulated 8 h after incubation.

2.3. Cloning

As the nucleotide sequence of medaka *rock1* was different from that currently available from the National Center of Biotechnology Information (NCBI) database

150 (https://www.ncbi.nlm.nih.gov/), the gene was subjected to cDNA cloning. The
151 nucleotide sequence of the *rock1* coding region was determined from follicle cDNA using
152 reverse transcription-polymerase chain reaction (RT-PCR) with KOD Fx DNA
153 polymerase (Toyobo; Osaka, Japan). The primers used were Rock1 pET SS and Rock1
154 cds-AS (Supplementary Table S1). The PCR products were phosphorylated, gel-purified,
155 and ligated into pBluescript SK vector (Agilent Technologies; Santa Clara, CA). The
156 nucleotide sequence of the resulting vector was confirmed by sequencing. The determined
157 sequence was deposited in the DDBJ/GenBank/NCBI database (Accession number:
158 LC726226).
159
160 **2.4. Reverse-transcription and real-time PCR**
161 Total RNA isolation, and real-time quantitative RT-PCR (qRT-PCR) were performed as
162 previously described (Ogiwara and Takahashi, 2016). The primer pairs used are listed in
163 Table S1. To determine the expression level, KOD SYBR qPCR Mix (Toyobo) or KAPA
164 Fast qPCR Kit (Nippon Genetics Co., Ltd.; Tokyo, Japan) was used. To normalize the
165 transcript levels of the target genes, we tested the housekeeping genes, such as
166 cytoplasmic actin (*actb*), 18S rRNA (*rn18s1*), ribosomal protein L7 (*rpl7*), and elongation
167 factor 1a (*eef1a*). The most stably expressed gene in the examined tissues was *eef1a*;

168 therefore, *eef1a* mRNA expression was used for normalization. The qPCR threshold cycle
169 (Ct) value was automatically determined using the instrument' software (Thermal Cycler
170 Dice, Real-Time System II software Ver.5.1.1, TAKARA BIO Inc., Shiga, Japan). The Δ
171 Ct value (Ct value of the reference sample minus Ct of the sample minus) was calculated,
172 and $2^{\Delta Ct}$ was calculated. The relative expression data were generated using the resulting
173 values.
174
175 **2.5. Antibody preparation**
176 Recombinant antigens were produced using *E. coli.* expression system. The coding
177 regions of Rhoa-a and Rhoa-c, or the partial coding region of Rock1 were amplified using
178 PCR with KOD Fx Neo DNA polymerase (Toyobo), and the primer pairs are listed in
179 Table S1. The PCR products were ligated into the pET 30a vector (Novagen; Madison,
180 WI), and the nucleotide sequences were confirmed by sequencing. The recombinant
181 proteins were expressed and purified as previously described (Ogiwara and Takahashi,
182 2007). The purify of the purified proteins was confirmed using SDS-PAGE. After
183 electrophoresis, the gel was stained with 0.25% Coomassie Brilliant Blue (CBB) in 30%
184 methanol, 10% acetic acid, and 40% H_2O. After staining for 20 min, the gel was destained
185 with 30% methanol, 10% acetic acid, and 40% H_2O. Specific antibodies were produced

186 in mice (Ogiwara et al., 2013) and purified (Ogiwara et al., 2012), according to previously
187 described methods. Mouse anti-medaka Rpl7 antibody was prepared as previously
188 described (Ogiwara and Takahashi, 2019).
189
190 **2.6. Tissue extract preparation, immunoprecipitation (IP), and western blot analysis**
191 Follicle extract for IP was prepared from 30 ovarian follicles per sample as previously
192 described (Ogiwara et al., 2021). The follicle layer extract was prepared as previously
193 described (Ogiwara et al., 2005). The protein concentration was determined using a BCA
194 kit (Thermo Fischer Scientific, San Jose, CA). IP and western blotting were performed as
195 previously described (Ogiwara et al., 2021), except that anti-medaka Rhoa-c or anti-
196 medaka Rock1 antibodies were used. We examined the protein expression of Actb,
197 Glyceraldehyde-3-phosphate dehydrogenase, and Rpl7 to select an appropriate protein as
198 a reference using the follicle layer and preovulatory follicle extract. The most stably
199 expressed protein in the examined tissues was Rpl7; therefore, Rpl7 was used as the
200 reference.
201
202 **2.7. Primary granulosa cell (pGC) preparation**
203 GCs were isolated from -1 h follicles, and pGCs were prepared according to a previously

described method (Ogiwara and Takahashi, 2016).

2.8. Immunohistochemistry

Paraffin sections (5 μm thick) were prepared as previously described (Ogiwara et al., 2015). The sections were dewaxed twice in xylene for 10 min and then placed in 99% ethanol for 2 min. The samples were hydrated using a graded ethanol series and then rinsed with pure water for 5 min. The specimens were then placed in phosphate-buffered saline (PBS) for 2 min and incubated in PBS containing 3% H_2O_2 for 10 min. The sections were then incubated in PBS containing 1% bovine serum albumin (Wako) at room temperature for 60 min and with anti-medaka Rhoa-c or Rock1 antibody diluted in PBS at room temperature for 60 min. They were then washed three times with PBS for 20 min and incubated with a DAKO envision mouse (Agilent Technologies Inc.) for 60 min. After washing three times with PBS for 20 min, the signal was detected using the ImmPACT™ AEC HRP Substrate kit (Vector Laboratories, Burlingame, CA). As a negative control, the primary antibody and its antigen (20 μg) were diluted in PBS, preincubated for 16 h at 4°C, and used for immunohistochemistry.

2.9. Active Rhoa-c detection

Active medaka Rhoa-c was detected using a RhoA Pull-Down Activation Assay Biochem Kit (Cytoskeleton Inc.) according to the manufacturer's instructions. For sample preparation, follicle layers from preovulatory follicles or follicles cultured with chemicals were homogenized in the cell lysis buffer supplied in the kit. The sample was then centrifuged at 12,000 ×g for 10 min, and the resulting supernatant was used for the assay. Active Rhoa-c was detected by western blot analysis using an anti-medaka Rhoa-c antibody.

2.10. *rhoa-c*, *rock1*, or *ptger4b* knockout in OLHNI-2 cells

The knockout was performed using CRISPR/Cas9-mediated genome editing according to a previous method (Ogiwara et al., 2021). Briefly, the oligonucleotide pair listed in Table S1 was annealed and ligated to pDR274, and a medaka caudal fin cell line (OLHNI-2) derived from the HNI strain, which was obtained from the RIKEN BioResource Center (Tsukuba, Japan), was co-transfected with the vector and Cas9 nuclease expression vector carrying a hygromycin B resistance gene. After hygromycin B selection, the cells were used for the experiments.

2.11. G-/F-actin detection

The G-/F-actin ratio was measured as previously described (Ogiwara and Takahashi, 2016). Briefly, OLHNI-2 cells and follicle layers from preovulatory follicles or follicles cultured with chemicals were gently homogenized in an actin stabilization buffer to prepare the G-actin and F-actin fractions. The samples were then subjected to western blot analysis. The actin bands were detected using an anti-medaka Actb antibody.

2.12. Statistical analysis

To validate our results, all experiments were repeated 3-8 times. The data collected were subjected to statistical analysis using Excel software, and the mean of 3-8 replicates was evaluated as the mean ± standard error of the mean. Significance was determined using Student’s t-test or one-way analysis of variance (ANOVA) followed by Dunnett's or Tukey's post hoc test, as appropriate, and presented as $P<0.05$ (*) or $P<0.01$ (**). Equal variation was confirmed using the F-test or Bartlett’s test as appropriate. For western blotting and immunohistochemical analyses, at least three separate experiments were performed to confirm the reproducibility of the findings, and the representative results of all experiments are shown.

3. Results

3.1. Rho inhibitor inhibits in vitro ovulation in medaka

Our previous study reported that Ptger4b activation did not activate or inhibit adenylate cyclase in the OLHNI2 cell line; thus, Ptger4b is strongly suggested to be coupled with G12/13 or Gq/G11 to activate the Ptger4b signaling pathway (Takahashi et al., 2018). This possibility was examined using in vitro follicle culture. It is well established that G12/13 proteins can couple with G-protein-coupled receptors to activate RHO by regulating the activity of RhoGTPase nucleotide exchange factors (Siehler, 2009; Vogt, 2003). We first examined whether RHO family protein(s), including RHO, CDC42, and RAC1 (Tapon and Hall, 1997), are involved in medaka ovulation. When -3 h follicles were cultured with or without each RHO family member inhibitor, in vitro ovulation was significantly inhibited by the RHO inhibitor (Fig. 1A). No significant inhibitory effects were observed in follicles treated with the CDC42 inhibitor ML141 or the RAC1 inhibitor. Ovulation was blocked in a dose-dependent manner by an RHO inhibitor (Fig. 1B). Incubating -3h follicles with GW627368X, an EP4 antagonist, strongly inhibited in vitro ovulation, which was ameliorated by adding the RHO activator (Fig. 1C). These results indicate that Rho acts in the Ptger4b signaling pathway and Rho activation is required for successful medaka ovulation.

3.2. Rho mRNA and protein expression in preovulatory follicles during a 24 h spawning cycle

As Rho is an important factor in the Ptger4b signaling pathway and medaka ovulation, a medaka genome database was searched using the Ensembl genome browser (Ensembl database, https://www.ensembl.org/index.html) to identify the *rho* gene(s) responsible for the Ptger4b signaling pathway. Six *rho* genes, *rhoa-a, rhoa-b*, *rhoa-c*,

282 *rhob*, *rhog*, and *rhou*, were identified. Real-time RT-PCR analysis of mRNAs of these
283 genes revealed that all the RNAs were present, with the highest expression for *rhoa-c* and
284 the second highest for *rhoa-a* in the follicle layers of the -3 h follicles (Fig. 2A). *rhoa-a*
285 and *rhoa-c* mRNA expression patterns in the preovulatory follicle during a 24 h spawning
286 cycle were examined. Both mRNAs were constitutively expressed in the follicles (Fig.
287 2B and C).

288 To detect Rho proteins in preovulatory follicles, we generated a mouse polyclonal
289 antibody raised against medaka Rhoa-a and Rhoa-c. Recombinant medaka Rhoa-a and
290 Rhoa-c were produced in an *E. coli* expression system and used separately as antigens for
291 immunization. The antibody cross-reacted with the respective antigens. However, the
292 antigen was not recognized by the absorbed antibody, indicating that the antibodies were
293 specific (Fig. 2D). The anti-Rhoa-c antibody detected the protein in the preovulatory
294 follicles; however, no bands were detected with the anti-Rhoa-a antibody (data not
295 shown). We further examined the expression of Rhoa-c in preovulatory follicles during a
296 24 h spawning cycle. The corresponding proteins associated with the preovulatory
297 follicles were detected by IP and western blotting using an antibody. The antibody
298 constitutively detected Rhoa-c, irrespective of when the extracts were prepared from
299 intact preovulatory follicles in the 24-h spawning cycle (Fig. 2E). Western blot analysis
300 revealed that Rhoa-c was expressed in GCs (Fig. 2F).

301 Immunohistochemical experiments using fish ovary sections collected 3 h before
302 ovulation were conducted to determine Rhoa-c localization, which showed the highest
303 mRNA expression in the -3 h-follicles in PCR analysis. Rhoa-c was localized in the
304 follicle layer of the largest or post-vitellogenic follicles (stage X; Fig. 2G, arrows and
305 asterisks) and was also expressed in the follicle layer of follicles larger than 150 μm,

306 which were in an early-, late-, or post-vitellogenic phase at stages V–IX (Fig. 2 G,
307 arrowheads). No signal was observed in the section stained with a pre-adsorbed
308 antibody/antigen complex, which was the antibody preincubated with its antigen
309 (absorbed antibody), indicating that the signal was specific (Fig. 2 G, lower panel). These
310 results indicate that Rhoa-c is expressed in the follicle layers of both vitellogenic and
311 post-vitellogenic follicles. These results also indicate that the Rho protein plays a role in
312 PGE_2/Ptger4b signaling in follicle layers.

313

314 **3.3. Active Rhoa-c detection in follicles about to ovulate**

315 To examine whether the PGE_2 pathway mediates Rho activation in medaka
316 preovulatory follicles, a pull-down assay was conducted to detect active Rho in the
317 follicles. Active Rhoa-c was pulled-down from the extracts and the precipitating Rhoa-c
318 was detected by western blot analysis. Active Rhoa-c was detected in the -3 and -1 h
319 follicles but not in the -6 h follicles (Fig. 3A). Rhoa-c was activated after incubating the
320 -3 h follicles with PGE_2 in vitro, which was inhibited by GW627368X. However, this
321 inhibitory effect was abolished by the addition of the Rho activator (Fig. 3B). No
322 inhibitory effects were observed when the follicles were cultured with Rho or Rock
323 inhibitors. These results indicate that Rhoa-c is activated downstream of Ptger4b.

324

325 **3.4. Rock involvement in medaka ovulation**

326 Rho exerts its biological effects by binding to its downstream effector molecules
327 including Rock, an important downstream factor. As active Rhoa-c was detected in
328 follicles about to ovulate, we examined whether Rock might be involved in medaka
329 ovulation. In vitro ovulation was significantly suppressed in a dose-dependent manner
330 after culturing preovulatory follicles with the Rock inhibitor, which was not abolished
331 after culturing the follicles with both the Rock inhibitor and Rho activator (Fig. 4A, B).
332 To predict the timing of Rock activation, we examined the in vitro ovulation rates after
333 exposing the follicles to the inhibitor for various time periods (Fig. 4C). Ovulation was
334 strongly inhibited when the follicles were cultured in the presence of Rock inhibitor for
335 8 h (-3 to +5 h), 7 h (-2 to +5 h), and 6 h (-1 to +5 h). Exposure of the follicles to the
336 inhibitor for 1 h (-3 to -2 h) or 2 h (-3 to -1 h) did not inhibit ovulation significantly. The
337 above results suggest that Rock is involved in medaka ovulation, and that kinase activity
338 is required for successful ovulation between -1 h and 0 h.

339

340 **3.5. Rock mRNA and protein expression in the preovulatory follicles during 24 h**
341 **spawning cycles**

342 A datadase search for medaka *rock* genes using the Ensembl genome database
343 revealed that the fish possessed three *rock* genes: *rock1, rock2a*, and *rock2b*. Among these
344 *rock* genes, *rock1* expression levels were highest in the follicle layers of -3 h follicles (Fig.

345 5A). Therefore, *rock1* was further analyzed by studying *rock1* mRNA expression in
346 preovulatory follicles using the total RNA extracted from intact follicles obtained from
347 the ovaries at various time points during the 24-h spawning cycle (Fig. 5B). The *rock1*
348 transcript levels were almost constant in the preovulatory follicles during the spawning
349 cycle.
350 A mouse polyclonal antibody for recombinant medaka Rock1 was prepared and its
351 specificity was confirmed (Fig. 5C). Western blot analysis was performed using follicle
352 layer extracts to detect Rock1 protein. The corresponding protein associated with the
353 follicle layer of the preovulatory follicles was detected using the antibody at position 158
354 kDa in all the extracts examined, corresponding to the size predicted for the medaka
355 Rock1 protein (Fig. 5D). Western blot analysis revealed that the Rock1 protein was
356 expressed in the GCs (Fig. 5E). In the immunohistochemical analysis of the fish ovary
357 sections 3 h before ovulation, the medaka Rock1 antibody detected positive signals
358 associated with the follicle layer of the largest follicle (stage X) (Fig. 5F, arrows and
359 asterisks). Signals were also detected in the follicle layer of follicles larger than 150 μm,
360 corresponding to the early-, late-, or post-vitellogenic phases (stages V–IX) (Fig. 5 F,
361 arrowheads). In stage X follicles, positive signals for Rock1 protein were localized in
362 GCs (Fig. 5 F, lower right panel). No signal was observed in the section stained with a

363 pre-adsorbed antibody/antigen complex, which was the antibody pre-incubated with the
364 antigen (absorbed antibody) (Fig. 5 F, upper right panel).
365
366 **3.6. PGE_2 modulates actin filament polymerization in the follicle cells of follicles**
367 **about to ovulate via the Rho/Rock pathway.**
368 Our previous studies suggested that the PGE_2/Ptger4b signaling cascade is involved
369 in intracellular actin cytoskeleton rearrangement in follicle cells of follicles about to
370 ovulate (Ogiwara and Takahashi, 2016; Takahashi et al., 2018). To examine whether the
371 Rho/Rock pathway is involved in actin filament rearrangement, we analyzed the actin
372 cytoskeleton polymerization status in follicle cells of follicles cultured with reagents that
373 affect the Rho/Rock pathway. The G-/F-actin ratio increased significantly when follicles
374 were cultured without any inhibitor. This increase was inhibited by GW627368X;
375 however, this inhibition was abolished by adding the Rho activator together with the
376 antagonist. The G-/F-actin ratio did not increase in follicles treated with Rho or Rock
377 inhibitor (Fig. 6A).
378 OLHNI-2 cells, which express Ptger4b, Rhoa-c, and Rock, were treated with PGE_2 to
379 examine the effects of these proteins on changes in rearrangement (Fig. 6B). The G-/F-
380 actin ratio significantly increased at 6 h after PGE_2 treatment. Next, we analyzed the ratio
381 of Rhoa-c-, Rock1-, and Ptger4b-deficient OLHNI-2 cells. No bands for Rhoa-c or Rock1
382 were detected in the knockout cells (Fig. 6C). We could not examine Ptger4b protein
383 expression in knockout cells, because a Ptger4b-specific antibody was not available. The
384 G-/F-actin ratio was significantly increased in PGE_2-treated cells, but not in PGE_2-treated
385 knockout cells (Fig. 6D).

These results indicate that PGE_2/Ptger4b and its downstream Rho/Rock system are involved in intracellular actin cytoskeleton rearrangement.

4. Discussion

We previously reported that the PGE_2/Ptger4b system is involved in medaka ovulation (Fugimori et al., 2011; Fugimori et al., 2012) and that PGE_2 exerts its effects through Ptger4b between -1 and 0 h of ovulation (Fugimori et al., 2012). Moreover, we have previously suggested that PGE_2/Ptger4b-mediated intracellular actin cytoskeleton rearrangement in follicles about to ovulate is important for medaka ovulation (Ogiwara and Takahashi, 2016; Takahashi et al., 2018). This study was conducted to further substantiate the role of the PGE_2/Ptger4b system in follicle ovulation and clarify the signaling cascade of the system. The results of this study strengthen the notion that intracellular actin cytoskeleton rearrangement in the GCs of ovulating follicles is necessary for successful ovulation in medaka. This study also revealed that PGE_2/Ptger4b system activation-induced changes in the cytoskeleton during ovulation are mediated via the Rho/Rock pathway.

The rationale for our conclusion that PGE_2/Ptger4b induces intracellular actin cytoskeleton rearrangement via the Rho/Rock pathway in the GCs of preovulatory follicles at ovulation is as follows: (i) Rhoa-c and Rock1 proteins were expressed in the

405 GCs of preovulatory follicles (Fig. 2F and 5E). (ii) Rhoa-c was activated in follicle cells
406 of follicles immediately before ovulation (Fig. 3). (iii) The G-/F-actin ratio increased in
407 the GCs of the follicles immediately before ovulation, and at or around the time of
408 ovulation in the control follicles. In contrast, treatment of preovulatory follicles with a
409 Ptger4b antagonist, Rho inhibitor, or Rock inhibitor suppressed in vitro follicle ovulation
410 and inhibited the increase in the G-/F-actin ratio (Fig. 1, 4, and 6). (iv) Rhoa-c was
411 activated and the G-/F-actin ratio increased during control follicle ovulation; however,
412 opposite results were noted in both events aftert GW627368X treatment. GW627368X-
413 mediated ovulation inhibition was abolished by further treatment with Rho activator (Fig.
414 1, 3, and 6). (v) The G-/F-actin ratio significantly increased in control OLHNI-2 cells
415 following treatment with PGE_2. However, this PGE_2-induced G-/F-actin ratio increase
416 was not detected in Ptger4b-, Rhoa-c-, or Rock1-deficient cells (Fig. 6). Based on these
417 results and our previous findings (Ogiwara and Takahashi, 2016), we proposed a pathway
418 for the induction of actin cytoskeleton rearrangement. PGE_2, secreted by GCs (Ogiwara
419 and Takahashi, 2016; Takahashi et al., 2018), activates Rhoa-c. Currently, the pathway
420 through which active Rock1 causes intracellular actin cytoskeleton rearrangement
421 remains unknown. In mammals, the LIM-Kinase (LIMK)/cofilin pathway (Venessa T
422 Chin et al., 2015), myosin light chain kinase (MLCK) (Sharanek et al., 2016), and ERM

423 (ezrin, radixin, moesin) proteins (Jiao et al., 2017), are reported to be activated by the
424 Rho/Rock pathway to regulate intracellular actin cytoskeleton rearrangement. We
425 examined whether these factors are involved in PGE_2-induced intracellular actin
426 cytoskeleton rearrangement in medaka ovulatory follicles. However, in vitro follicle
427 ovulation was not significantly inhibited when follicles were cultured with LIMK or
428 MLCK inhibitors (data not shown). Ogiwara and Takahashi (2016) reported that moesin
429 A is involved in the regulation of intracellular actin cytoskeleton rearrangement. In the
430 present study, GW627368X did not inhibit moesin A phosphorylation (data not shown),
431 suggesting that moesin A is not a downstream target of Rock1 (Ogiwara and Takahashi,
432 2016). We speculate that there is a novel pathway for inducing actin filament
433 rearrangement that involves factor(s) other than LIMK/Coffin, MLCK, and ERM proteins
434 downstream of Rock1 in medaka ovarian follicles.

435 Pendergrass and Schroeder (1976), Jalabert and Szöllösi (1975), and Trubnikova
436 (2003) reported that cytochalasin B, an actin polymerization inhibitor, inhibits ovulation
437 in medaka, trout, and sturgeons, respectively. Thus, actin cytoskeleton rearrangement
438 accompanying ovulatory processes may be common among teleosts. However, the
439 mechanism underlaying cytochalasin-B-mediated teleost ovulation inhibition remains
440 unclear. However, the results reported by Ogiwara and Takahashi (2016) and those of the

present study provide information that answers this long-standing question. An alteration in the extent of actin polymerization within follicle cells, particularly in GCs, is required for LH-induced ovulation; therefore, a disturbance of actin cytoskeleton rearrangement by cytochalasin B treatment most likely causes anovulation. Studies on follicle rupture during ovulation in medaka have established that successful ovulation is assured by the activation of two events induced after the LH surge: ECM protein hydrolysis in the follicle layers of ovulating follicles (Ogiwara et al., 2005; Takahashi et al., 2019) and actin cytoskeleton rearrangement in GCs (Fujimori et al., 2011; Fujimori et al., 2012; Hagiwara et al., 2014; Ogiwara and Takahashi, 2016). The removal of ECM proteins surrounding the GCs by proteolytic enzymes and changes in the intracellular actin cytoskeleton in GCs disintegrates cell-cell interactions in GCs, oocytes, and neighboring GCs. This probably increases GC mobility, facilitating the formation of openings in the apical region through which the oocyte can escape from the periovulatory follicles.

In summary, the results of this study revealed that actin cytoskeleton rearrangement is regulated by the PGE_2/Ptger4b system via the Rho/Rock pathway. Although several studies have implicated intracellular actin cytoskeleton in teleost ovulation, its physiological relevance remains unclear. This study is the first to report that Rhoa-c/Rock1 regulates actin cytoskeleton rearrangement during ovulatory processes in

459 medaka. Further studies should focus on identifying additional factors involved in PGE_2-
460 induced actin cytoskeleton rearrangement during ovulation to fully understand the
461 signaling pathways and regulatory mechanisms of this process.
462

463 **Acknowledgements**

464 This work was supported by Grants-in-Aid for Scientific Research (16H04810 to TT and
465 15K07120 to KO) from the Ministry of Education, Culture, Sports, Science and
466 Technology of Japan.
467
468

469 References

470 Bradley, J., A., Goetz, F., W., 1994. The inhibitory effects of indomethacin,
471 nordihydroguaiaretic acid, and pyrrolidinedithiocarbamate on ovulation and
472 prostaglandin synthesis in yellow perch (Perca flavescens) follicle incubates.
473 Prostaglandins 48, 11–20.
474

475 Baker, S.J.C., Corrigan, E., Melnyk, N., Hilker, R., Van Der Kraak, G. 2021. Nuclear
476 progesterone receptor regulates ptger4b and PLA2G4A expression in zebrafish (Danio
477 rerio) ovulation. Gen. Comp. Endocrinol. 311, 113842
478

479 Baker, S.J.C. Van der Kraak, G. 2019. Investigating the role of prostaglandin receptor
480 isoform EP4b in zebrafish ovulation. Gen. Comp. Endocrinol. 283, 113228.

Christenson, L.K., Gunewardena, S., Hong, X., Spitchak, M., Baufeld, A., Vanselow, J., 2013. Research resource: preovulatory LH surge effects on follicular theca and granulosa transcriptomes. Mol. Endocrinol. 27, 1153–1171.

Davis, B.J., Lennard, D.E., Lee, C.A., Tian, H.F., Morham, S.G., Wetsel, W.C., Langenbach, R., 1999. Anovulation in cyclooxygenase-2-deficient mice is restored by prostaglandin E2 and interleukin-1β. Endocrinology 140, 2685–2695.

Diao, G., Huang, J., Zheng, X., Sun, X., Tian, M., Han, J., Guo, J., 2021. Prostaglandin E2 serves a dual role in regulating the migration of dendritic cells. Int. J. Mol. Med. 47(1), 207–218.

Duffy, D.M, Ko, C., Jo, M., Brannstrom, M., Curry, T.E. 2019. Ovulation: Parallels with inflammatory processes. Endocr. Rev. 40(2): 369–416.

Ensembl genome browser, http://www.ensembl.org/index.html (Release 106) (accessed 1 July 2022).

Espey, L.L., Richards, J.S., 2002. Temporal and spatial patterns of ovarian gene transcription following an ovulatory dose of gonadotropin in the rat. Biol. Reprod. 67, 1662–1670.

503

504 Espey, L.L., Richards, J.S., 2006. Ovulation. In: Neill JD, editor. Physiology of

505 Reproduction, 3rd edition. Amsterdam: Academic Press. 425–474.

506

507 Fujimori, C., Ogiwara, K., Hagiwara, A., Rajapakse, S., Kimura, A., Takahashi, T., 2011.

508 Expression of cyclooxygenase-2 and prostaglandin receptor EP4b mRNA in the ovary of

509 the medaka fish, *Oryzias latipes*: Possible involvement in ovulation. Mol. Cell.

510 Endocrinol. 332 (1-2), 67–77.

511

512 Fujimori, C., Ogiwara, K., Hagiwara, A., Takahashi, T., 2012. New evidence for the

513 involvement of prostaglandin receptor EP4b in ovulation of the medaka, *Oryzias latipes*.

514 Mol. Cell. Endocrinol. 362 (1-2), 76–84.

515

516 Gilbert, I., Robert, C., Dieleman, S., Blondin, P., Sirard, M.A., 2011. Transcriptional

517 effect of the LH surge in bovine granulosa cells during the peri-ovulation period.

518 Reproduction 141, 193–205.

519

520 Hagiwara, A., Ogiwara, K., Katsu, Y., Takahashi, T., 2014. Luteinizing Hormone-Induced

521 Expression of Ptger4b, a Prostaglandin E2 receptor indispensable for ovulation of the

522 Medaka Oryzias latipes, is regulated by a genomic mechanism involving nuclear

523 progestin receptor. Biol. Reprod. 90(6), 126, 1-14.

524

525 Hizaki, H., Segi, E., Sugimoto, Y., Hirose, M., Saji, T., Ushikubi, F., Matuoka, T., Noda,
526 Y., Tanaka, T., Yoshida, N., Narumiya, S., Ichikawa, A., 1999. Abortive expansion of the
527 cumulus and impaired fertility in mice lacking the prostaglandin E receptor subtype EP(2).
528 Proc. Natl. Acad. Sci. U. S. A. 96, 10501–10506.

529

530 Jalabert, B., Szollosi, D., 1975. In vitro ovulation of trout oocytes: effect of prostaglandins
531 on smooth muscle-like cells of the theca. Prostaglandins 9, 765–778.

532

533 Jiao, X., Ashtari, N., Rahimi-Balaei, M., Chen, Q.M., Badbezanchi, I., Shojaei, S.,
534 Marzban, A., Mirzaei, N., Chung, S., Guan, T., Li, J., Vriend, J., Mehr, S.E., Kong, J.,
535 Marzban, H., 2017. Mevalonate Cascade and Neurodevelopmental and
536 Neurodegenerative Diseases: Future Targets for Therapeutic Application. Curr. Mol.
537 Pharmacol. 10 (2), 115–140.

538

539 Kagawa, H., Tanaka, H., Unuma, T., Ohta, H., Gen, K., Okuzawa, K., 2003. Role of
540 prostaglandin in the control of ovulation in the Japanese eel *Anguilla japonica*. Fish. Sci.
541 69, 234–241.

542

543 Kennedy, C.R., Zhang, Y., Brandon, S., Guan, Y., Coffee, K., Funk, C.D., Magnuson,

544 M.A., Oates, J.A., Breyer, M.D., Breyer, R.M., 1999. Salt-sensitive hypertension and
545 reduced fertility in mice lacking the prostaglandin EP2 receptor. Nat. Med. 5, 217–220.
546
547 Kim, S.O., Duffy, D.M., 2016. Mapping PTGERs to the ovulatory follicle: regional
548 responses to the ovulatory PGE_2 signal. Biol. Reprod. 95 (33), 1–11.
549
550 Lister, A.L., Van Der Kraak G., 2008. An investigation into the role of prostaglandins in
551 zebrafish oocyte maturation and ovulation. Gen. Comp. Endocrinol. 159, 46-57.
552
553 Lubzens, E., G. Young, J. Bobe, J. Cerda, 2010. Oogenesis in teleosts: How fish eggs are
554 formed. Gen. Comp. Endocrinol. 165, 367-89.
555
556 Lussier, J.G., Diouf, M.N., Levesque, V., Sirois, J., Ndiaye, K., 2017. Gene expression
557 profiling of upregulated mRNAs in granulosa cells of bovine ovulatory follicles following
558 stimulation with hCG. Reprod. Biol. Endocrinol. 15, 88.
559
560 Martineau, L.C., McVeigh, L.I., Jasmin, B.J., Kennedy, C.R.J., 2004. p38 MAP kinase
561 mediates mechanically induced COX-2 and PG EP4 receptor expression in podocytes:

562 implications for the actin cytoskeleton. Am. J. Physiol. Renal. Physiol. 286(4), F693–701.

563

564 Najm, P., El-Sibai, M., 2014. Palladin regulation of the actin structures needed for cancer

565 invasion. Cell Adh. Migr. 8(1), 29–35.

566

567 NCBI database, https://www.ncbi.nlm.nih.gov/ (accessed 1 July 2022).

568

569 Ogiwara, K., Takano, N., Shinohara, M., Murakami, M., Takahashi, T., 2005. Gelatinase

570 A and membrane-type matrix metalloproteinases 1 and 2 are responsible for follicle

571 rupture during ovulation in the medaka. Proc. Natl. Acad. Sci. USA 102, 8442–8447.

572

573 Ogiwara, K., Takahashi, T., 2007. Specificity of the medaka enteropeptidase serine

574 protease and its usefulness as a biotechnological tool for fusion-protein cleavage. Proc.

575 Natl. Acad. Sci. USA 104 (17), 7021–7026.

576

577 Ogiwara, K., Minagawa, K., Takano, N., Kageyama, T., Takahashi, T., 2012. Apparent

578 Involvement of Plasmin in Early-Stage Follicle Rupture During Ovulation in Medaka.

579 Biol. Reprod. 86 (4) 113, 1–10.

580

581 Ogiwara, K. Fujimori, C. Rajapakse, S. Takahashi, T. 2013. Characterization of
582 Luteinizing Hormone and Luteinizing Hormone Receptor and Their Indispensable Role
583 in the Ovulatory Process of the Medaka. PLOS ONE Doi: 10.1371/journal.pone.0054482.

584

585 Ogiwara, K., Hagiwara, A., Rajapakse, S., Takahashi, T., 2015. The Role of Urokinase
586 Plasminogen Activator and Plasminogen Activator Inhibitor-1 in Follicle Rupture During
587 Ovulation in the Teleost Medaka. Biol. Reprod. 92 (1), 10.

588

589 Ogiwara, K., Takahashi, T., 2016. A Dual Role for Melatonin in Medaka Ovulation:
590 Ensuring Prostaglandin Synthesis and Actin Cytoskeleton Rearrangement in Follicular
591 Cells. Biol. Reprod. 94 (3), 64.

592

593 Ogiwara K., Takahashi, T., 2019. Nuclear Progestin Receptor Phosphorylation by Cdk9
594 Is Required for the Expression of Mmp15, a Protease Indispensable for Ovulation in
595 Medaka. Cells 8 (3), E215.

596

597 Ogiwara, K., Hoyagi, M., Takahashi, T., 2021. A central role for

598 cAMP/EPAC/RAP/PI3K/AKT/CREB signaling in LH-induced follicular Pgr expression
599 at medaka ovulation. Biol. Reprod. 105 (2), 413–426.
600
601 Pendergrass, P.C., Schroeder, P., 1976. The ultrastructure of the thecal cell of the teleost,
602 Oryzias latipes, during ovulation in vitro. J. Reprod. Fertil. 47, 229–233.
603
604 Richards, J.S., 1997. Sounding the alarm-does induction of prostaglandin endoperoxide
605 synthase-2 control the mammalian ovulatory clock? Endocrinology, 138, 4047–4048
606
607 Richards, J.S., 2007. Genetics of ovulation. Semin. in Reprod. Med. 25, 235–242.
608
609 Richards, J.S., Liu, Z., Shimada, M., 2015. Ovulation. In Knobil and Neill's Physiology
610 of Reproduction (edn) 4, 997–1021. Eds Plant T.M., Zeleznik, A.J., Amsterdam:
611 Academic Press.
612
613 Ridley, A.J., 2001. Rho GTPases and cell migration. J. Cell Sci. 114, 2713–2722.
614
615 Sena, J., Liu, Z., 2008. Expression of cyclooxygenase genes and production of

616 prostaglandins during ovulation in the ovarian follicles of Xenopus laevis. Gen. Comp.
617 Endocrinol. 157, 165–173.
618
619 Sharanek, A., Burban, A., Burbank, M., Guevel, R.L., Li, R., Guillouzo, A., Guguen-
620 Guillouzo, C., 2016. Rho-kinase/myosin light chain kinase pathway plays a key role in
621 the impairment of bile canaliculi dynamics induced by cholestatic drugs. Scientific
622 Reports 6, 24709.
623
624 Shimada, K., Olson, D.M., Etches, R.J., 1986. The effect of indomethacin on ovarian
625 prostaglandin release in hens. Biol. Reprod. 35, 1147–1153.
626
627 Siehler, S., 2009. Regulation of RhoGEF proteins by G12/13-coupled receptors. Br. J.
628 Pharmacol. 158 (1), 41–49.
629
630 Sorensen, P.W., Goetz, F.W., 1993. Pheromonal and reproductive function of F
631 prostaglandins and their metabolites in teleost fish. J. Lipid Mediat. 6, 385–393.
632
633 Takahashi, T., Fujimori, C., Hagiwara, A., Ogiwara, K., 2013. Recent advances in the
634 understanding of teleost medaka ovulation: the roles of proteases and prostaglandins.

635 Zoolog. Sci. 30 (4), 239–247.

636

637 Takahashi, T., Hagiwara, A., Ogiwara, K., 2018. Prostaglandins in teleost ovulation: A
638 review of the roles with a view to comparison with prostaglandins in mammalian
639 ovulation. Mol. Cell. Endocrinol. 461, 236–247.

640

641 Takahashi, T., Hagiwara, A., Ogiwara, K., 2019. Follicle rupture during ovulation with an
642 emphasis on recent progress in fish models. Reproduction 157 R1–R13.

643

644 Tang, H., Liu, Y., Li, J., Yin, Y., Li, G., Chen, Y., Li, S., Zhang, Y., Lin, H., Liu, X., Cheng,
645 C.H.K. 2016. Gene knockout of nuclear progesterone receptor provides insights into the
646 regulation of ovulation by LH signaling in zebrafish. Sci. Rep. 6, 28545.

647

648 Tapon, N., Hall, A., 1997. Rho, Rac and Cdc42 GTPases regulate the organization of the
649 actin cytoskeleton. Curr. Opin. Cell Biol. 9 (1), 86–92.

650

651 Tilley, S.L., Audoly, L.P., Hicks, E.H., Kim, H.S., Flannery, P.J., Coffman, T.M., Koller,
652 B.H., 1999. Reproductive failure and reduced blood pressure in mice lacking the EP2
653 prostaglandin E2 receptor. J. Clin. Invest., 103, 1539–1545.

654

655 Trubnikova, O.B., 2003. Effects of cycloheximide, aminoglutethimide, indomethacin,
656 cytochalasin B and colchicine on ovulation and the ultrastructure of the ovarian follicle
657 wall in the stellate sturgeon *Acipenser stellatus Pall*. Ontogenez 34 (2), 142–153.

658

659 van Helden, S.F.G., Oud, M.M., Joosten, B., Peterse, N., Figdor, C.G., van Leeuwen, F.N.,
660 2008. PGE2-mediated podosome loss in dendritic cells is dependent on actomyosin
661 contraction downstream of the RhoA–Rho-kinase axis. J. Cell Sci. 121 (7), 1096–1106.

662

663 Venessa T Chin, V.T., Nagrial, A.M., Chou, A., Biankin, A.V., Gill, A.J., Timpson, P.,
664 Pajic M., 2015. Rho-associated kinase signalling and the cancer microenvironment: novel
665 biological implications and therapeutic opportunities. Expert Rev. Mol. Med. 17:e17.

666

667 Vogt, S., Grosse, R., Schultz, G., Offermanns, S., 2003. Receptor-dependent RhoA
668 Activation in G12/G13-deficient Cells. GENETIC EVIDENCE FOR AN
669 INVOLVEMENT OF Gq/G11. J. Biol. Chem. 278, 28743–28749.

670

671 Yamaguchi, H., Condeelis, J., 2007. Regulation of the actin cytoskeleton in cancer cell
672 migration and invasion. Biochim. Biophys. Acta. 1773, 642–52.

673

674 Figure legends

675 **Fig. 1. Effects of RHO inhibitor, ML141, and RAC inhibitor on in vitro ovulation in**
676 **preovulatory follicles.** (A) The -3 h follicles were cultured for 8 h in the presence of Rho
677 inhibitor (Rho-i), ML 141, or Rac1 inhibitor (Rac1-i), and the ovulation rates were
678 determined. **P<0.01 (ANOVA and Dunnett's post hoc test, N =6). (B) The -3 h follicles
679 were cultured with Rho inhibitor at the indicated concentration. The ovulation rates were
680 determined after incubating for 8 h. *P<0.05, **P<0.01 (ANOVA and Dunnett's post hoc
681 test, N=6). (C) The -3 h follicles were cultured with GW627368X (GW) or both GW and
682 Rho activator (Rho-act). The ovulation rates were determined after incubating for 8 h.
683 **P<0.01 (ANOVA and Dunnett's post hoc test, N=6).

684

685 **Fig. 2. *rho*/Rho expression in medaka ovary.** (A) Real-time RT-PCR analysis was
686 conducted for *rho* genes using total RNA purified from the follicle layers isolated from
687 the preovulatory follicles 3 h before ovulation. (N=3). (B and C) Real-time RT-PCR
688 analysis was conducted for (B) *rhoa-a* and (C) *rhoa-c* using total RNA purified from the
689 preovulatory follicles isolated from ovaries at the indicated time points (N=5-7). (D)
690 Specificity of the antibodies for medaka Rhoa-a (left) and Rhoa-c (right) were examined.
691 Recombinant proteins for antigen were analyzed using CBB staining (CBB) or western
692 blot analysis using purified (WB) or recombinant protein-pretreated (WB(abs))
693 antibodies (left panels in each set). (E) Rhoa-c was detected by
694 immunoprecipitation/western blotting. As a negative control, -3 h follicle extract was
695 immunoprecipitated using normal mouse IgG bound to protein G-sepharose. The arrow
696 indicates Rhoa-c, and the asterisk denotes the band corresponding to the antibody used

for immunoprecipitation. As a positive control, Rpl7 was detected using the input fractions. (F) Rhoa-c was detected by western blotting using the extracts prepared from follicular layer (FL) and pGC. Rpl7 was used as a loading control. (G) Immunohistochemical analyses were performed in sections of the -3 h ovary. Purified anti-medaka Rhoa-c antibody (upper and middle panels) or the antibody previously treated with recombinant Rhoa-c (absorbed antibody) was used as a control (lower panel). The area indicated by a box in the upper panel is displayed at higher magnification in the middle panel. The follicle layer (arrows) of large preovulatory follicles (*) and the follicle layer (arrowheads) of medium-size follicles are positively stained. A representative result of four independent experiments is shown. Bars =300 μm in the upper and lower panels and 100 μm in the middle panel.

Fig. 3. Detection of active Rhoa-c in the follicle layer of preovulatory follicles and the follicles cultured with GW, Rho inhibitor, Rho-associated protein kinase inhibitor, and Rho-activator. (A) Active Rhoa-c was detected in follicle layer extracts prepared at the indicated time points. (B) The -6 h follicles were cultured with no additives for 0 h (-6 h layer), 3 h (Cont (3 h)), or 6 h (Cont (6 h)). The -6 h follicles were cultured with GW, Rho inhibitor (Rho-i), Rho-associated protein kinase (Rock) inhibitor (Rock-i), or both GW and Rho-activator for 6 h and then used to detect active Rhoa-c. Extracts of (A) -1 h or (B) -6 h follicle layers were boiled for 10 min and used as a negative control (Rtn). Active Rhoa-c was pulled-down from the extracts and the precipitating Rhoa-c was detected by western blot analysis. Arrows indicate signals for active Rhoa-c. Total Rhoa-c protein (control) was detected using the input fractions.

721 **Fig. 4. Effects of Rho-associated protein kinase (Rock) inhibitor on in vitro ovulation**
722 **in preovulatory follicles.** (A) The -3 h follicles were cultured with Rock inhibitor Y-
723 27632, and the ovulation rates were determined after incubating for 8 h. **P<0.01
724 (ANOVA and Dunnett's post hoc test, N=6). (B) The -3 h follicles were cultured with
725 Rock inhibitor or both the inhibitor and Rho activator (Rho-act). The ovulation rates were
726 determined after incubating for 8 h. **P<0.01 (ANOVA and Dunnett's post hoc test, N=6).
727 (C) The -3 h follicles were cultured with the inhibitor. Black bars and straight lines denote
728 the duration of follicle incubation with or without the inhibitor, respectively (left). The
729 ovulation rates were determined after incubation for 8 h. **P<0.01 (ANOVA and
730 Dunnett's post hoc test, N=6).
731
732 **Fig. 5. *rock1*/Rock1 expression in the medaka ovary.** (A) Real-time RT-PCR analysis
733 was conducted for *rock* genes using total RNA purified from the follicle layers isolated
734 from the follicles 3 h before ovulation. (N=3). (B) Real-time RT-PCR analysis was
735 conducted for *rock1* using total RNA purified from the preovulatory follicles isolated
736 from ovaries at the indicated time points (N=5-7). (C) Specificity of the antibody for
737 medaka Rock1 were examined. Recombinant protein for antigen was analyzed using CBB
738 staining (CBB) or western blot analysis using purified (WB) or recombinant protein-
739 pretreated (WB(abs)) antibodies. (D) Rock1 was detected by western blot analysis using
740 the extract purified from the follicle layer of preovulatory follicles isolated at the indicated
741 time points. Rpl7 was used as a loading control. (E) Rock1 was detected by western
742 blotting using the extracts prepared from follicular layer (FL) and pGC. Rpl7 was used as
743 a loading control. (F) Immunohistochemical analyses were performed in sections of the -
744 3 h ovary. Purified anti-medaka Rock1 antibody (two left and lower right panels) or the

745 antibody previously treated with recombinant Rock1 (absorbed antibody) was used as a
746 control (upper right panel). The area indicated by a box in the upper left panel is displayed
747 at higher magnification in the lower left panel. The area indicated by a box in the lower
748 left panel is displayed at further higher magnification in the lower right panel. The follicle
749 layer (arrows) of large preovulatory follicles (*) and the follicle layer (arrowheads) of
750 medium-size follicles were positively stained. TC, theca cell; GC, granulosa cell; OM,
751 oocyte membrane. A representative result of four independent experiments is shown. Bars
752 =300 μm in the two upper panels and 100 μm in the lower left panel.
753
754 **Fig. 6. The G-/F-actin ratio in the GCs of the preovulatory follicle or OLNI-2 cell.**
755 (A) The -4h follicles were incubated with GW627368X (GW), Rho inhibitor (Rho-i),
756 Rock inhibitor (Rock-i), or with both GW and Rho-activator for 4 h. Follicles cultured
757 without additives (-4 h layer and Cont) were also used as controls. After incubation for 4
758 h, G-actin and F-actin in the follicular layers were detected (lower two panels), and the
759 signal intensities of the bands were densitometrically quantified to determine the G-/F-
760 actin ratio. *P<0.05 (ANOVA and Dunnett's post hoc test, N=4). (B) OLHNI-2 cells were
761 treated with 100 nM PGE_2, and G-/F-actin ratio was determined. *P<0.05 (ANOVA and
762 Dunnett's post hoc test, N=4). (C) Rhoa-c (left) and Rock1 (right) were detected by
763 western blotting using the extracts of OLHNI-2 cell (Cont), or cells without medaka
764 Rhoa-c (Rhoa-c KO) or Rock1 (Rock1 KO). Rpl7 was used as a loading control. (D)
765 OLHNI-2 cells without medaka Rhoa-c (Rhoa-c KO), Rock1 (Rock1 KO), or Ptger4b
766 (Ptger4b KO) were cultured with or without 100 nM PGE_2 and G-/F-actin ratio was
767 determined as in (A). *P<0.05 (t-test, N=3).

Fig. 1

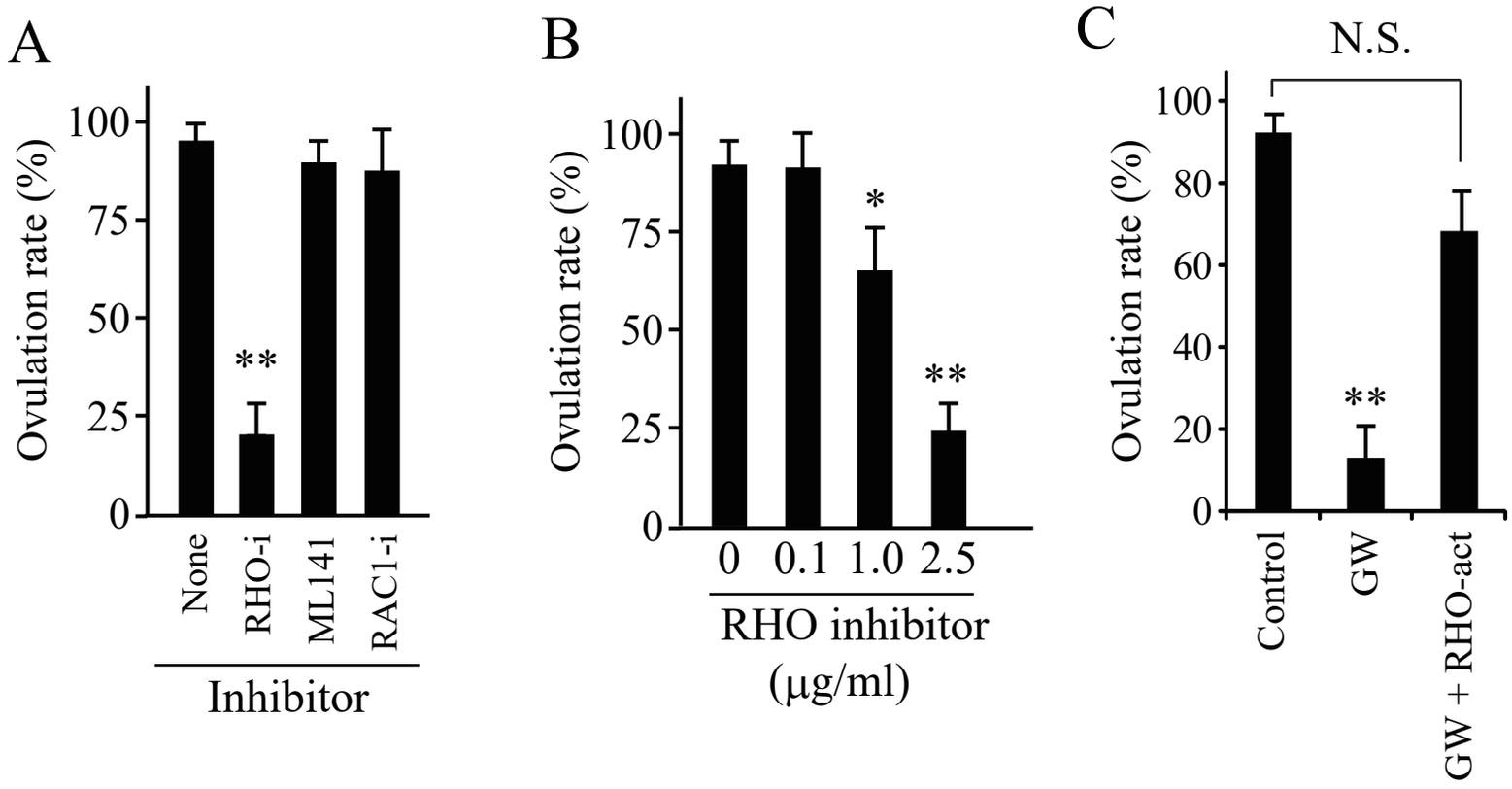
A
Ovulation rate (%)
100
75
50
25
0
**
None
RHO-i
ML141
RAC1-i
Inhibitor
B
Ovulation rate (%)
100
75
50
25
0
*
**
0
0.1
1.0
2.5
RHO inhibitor
(μg/ml)
C
N.S.
Ovulation rate (%)
100
80
60
40
20
0
**
Control
GW
GW + RHO-act

Fig. 2

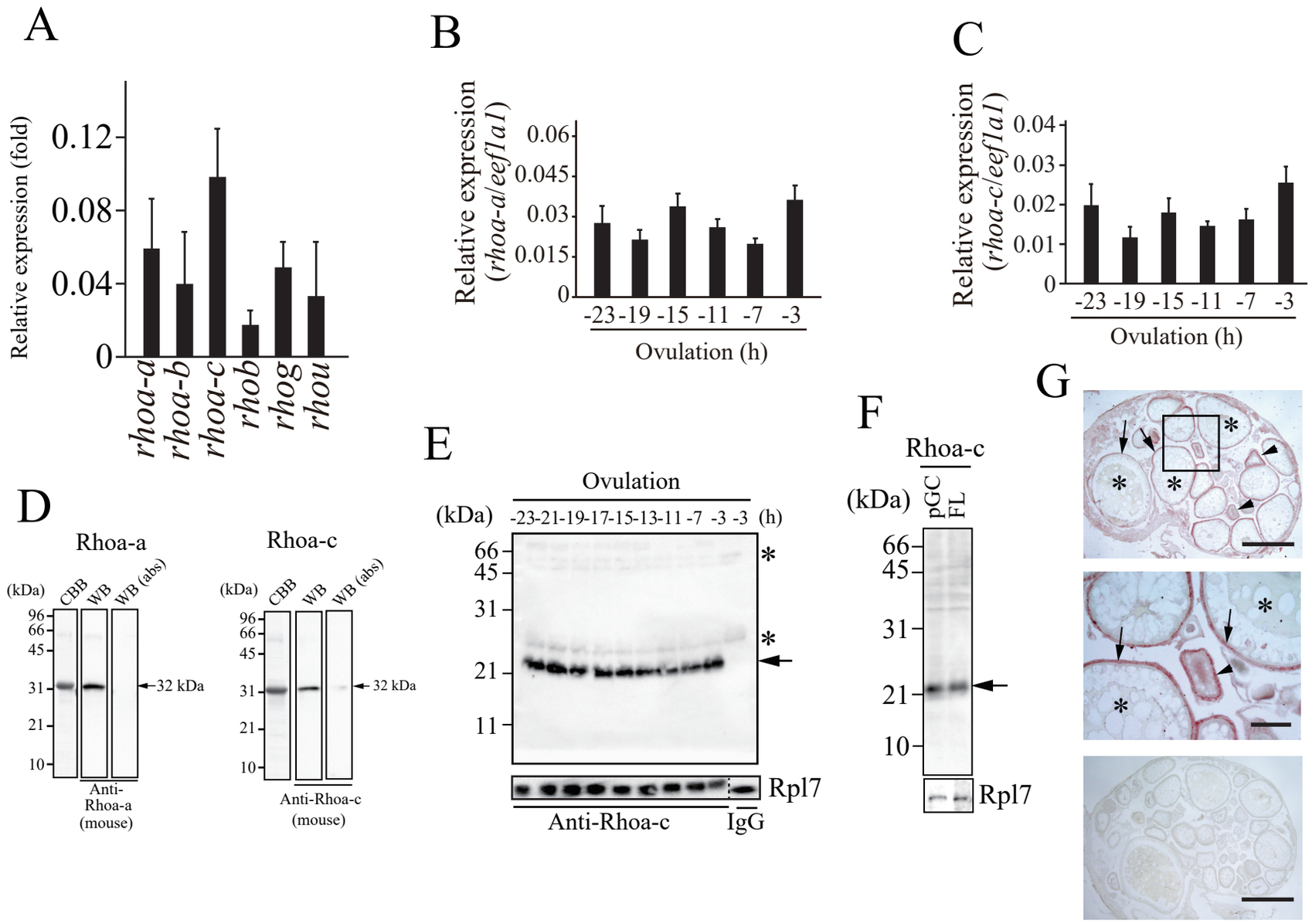
A
Relative expression (fold)
0.12
0.08
0.04
0
rhoa-a
rhoa-b
rhoa-c
rhob
rhog
rhou
B
Relative expression (rhoa-a/eef1a1)
0.06
0.045
0.03
0.015
0
-23 -19 -15 -11 -7 -3
Ovulation (h)
C
Relative expression (rhoa-c/eef1a1)
0.04
0.03
0.02
0.01
0
-23 -19 -15 -11 -7 -3
Ovulation (h)
D
Rhoa-a
(kDa)
CBB
WB
WB (abs)
96
66
45
31
21
10
32 kDa
Anti-Rhoa-a (mouse)
Rhoa-c
(kDa)
CBB
WB
WB (abs)
96
66
45
31
21
10
32 kDa
Anti-Rhoa-c (mouse)
E
Ovulation
(kDa)
-23-21-19-17-15-13-11 -7 -3 -3 (h)
66
45
31
21
11
*
*
Rpl7
Anti-Rhoa-c
IgG
F
Rhoa-c
(kDa)
pGC
FL
66
45
31
21
10
Rpl7
G
*
*
*
*
*

Fig. 3

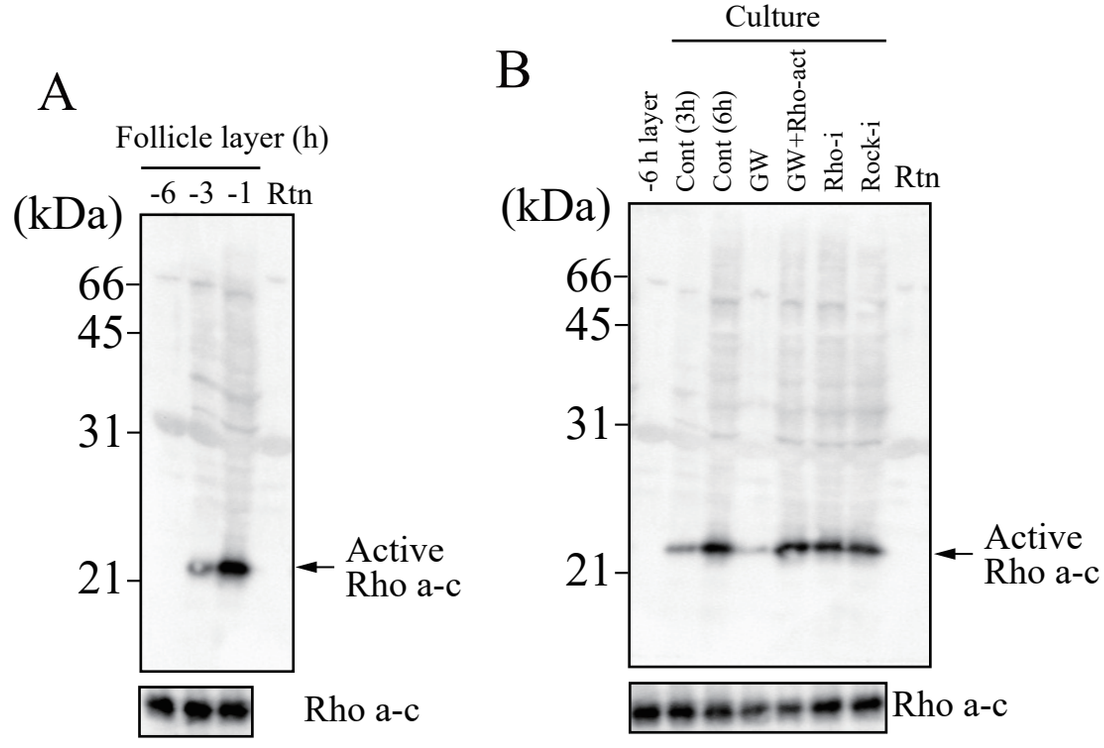
A
Follicle layer (h)
-6 -3 -1 Rtn
(kDa)
66
45
31
21
Active
Rho a-c
Rho a-c
B
Culture
-6 h layer
Cont (3h)
Cont (6h)
GW
GW+Rho-act
Rho-i
Rock-i
Rtn
(kDa)
66
45
31
21
Active
Rho a-c
Rho a-c

Fig. 4

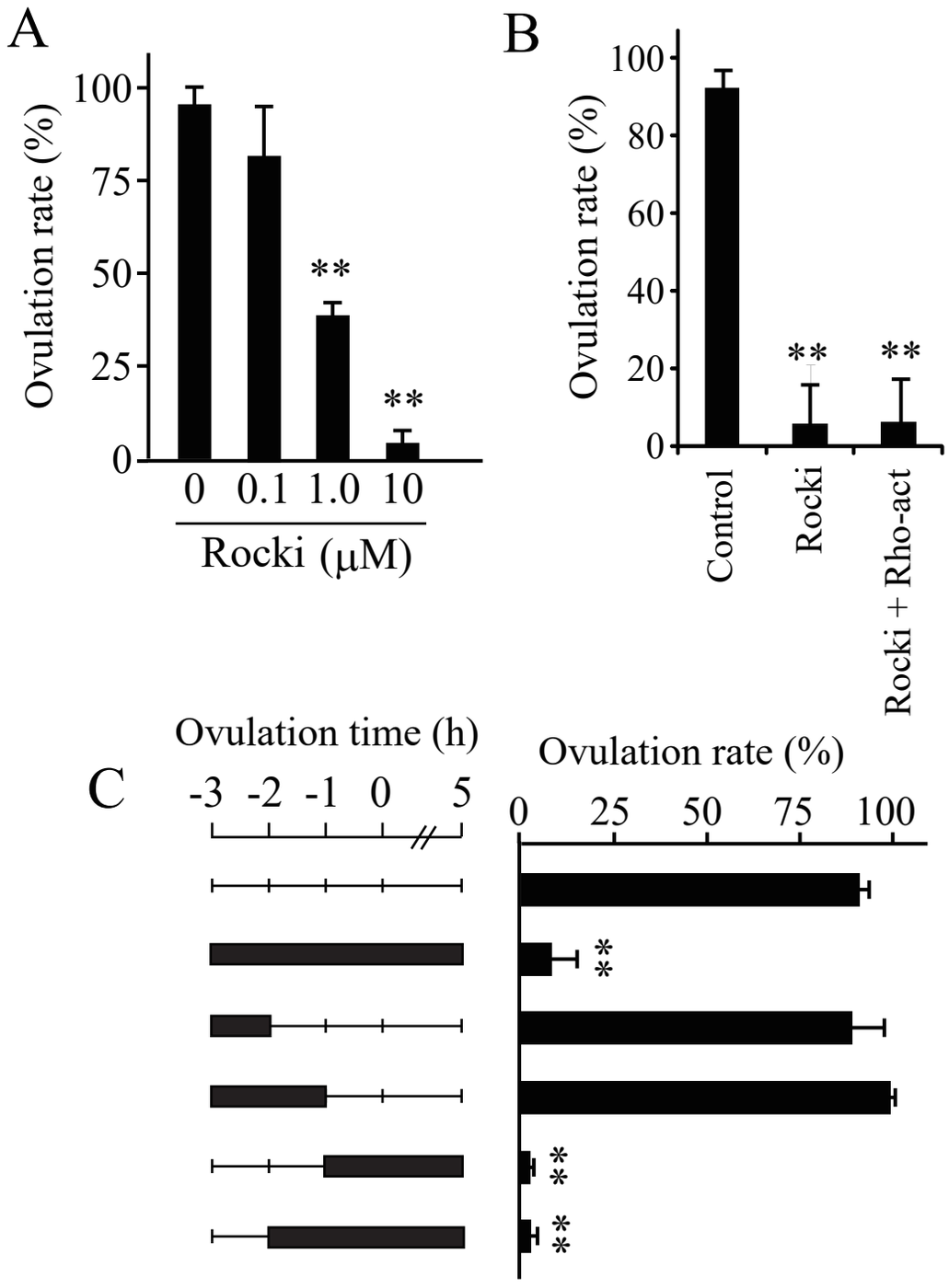
A
Ovulation rate (%)
100
75
50
25
0
**
**
0 0.1 1.0 10
Rocki (μM)
B
Ovulation rate (%)
100
80
60
40
20
0
**
**
Control
Rocki
Rocki + Rho-act
C
Ovulation time (h)
-3 -2 -1 0 5
Ovulation rate (%)
0 25 50 75 100
**
**
**

Fig. 5

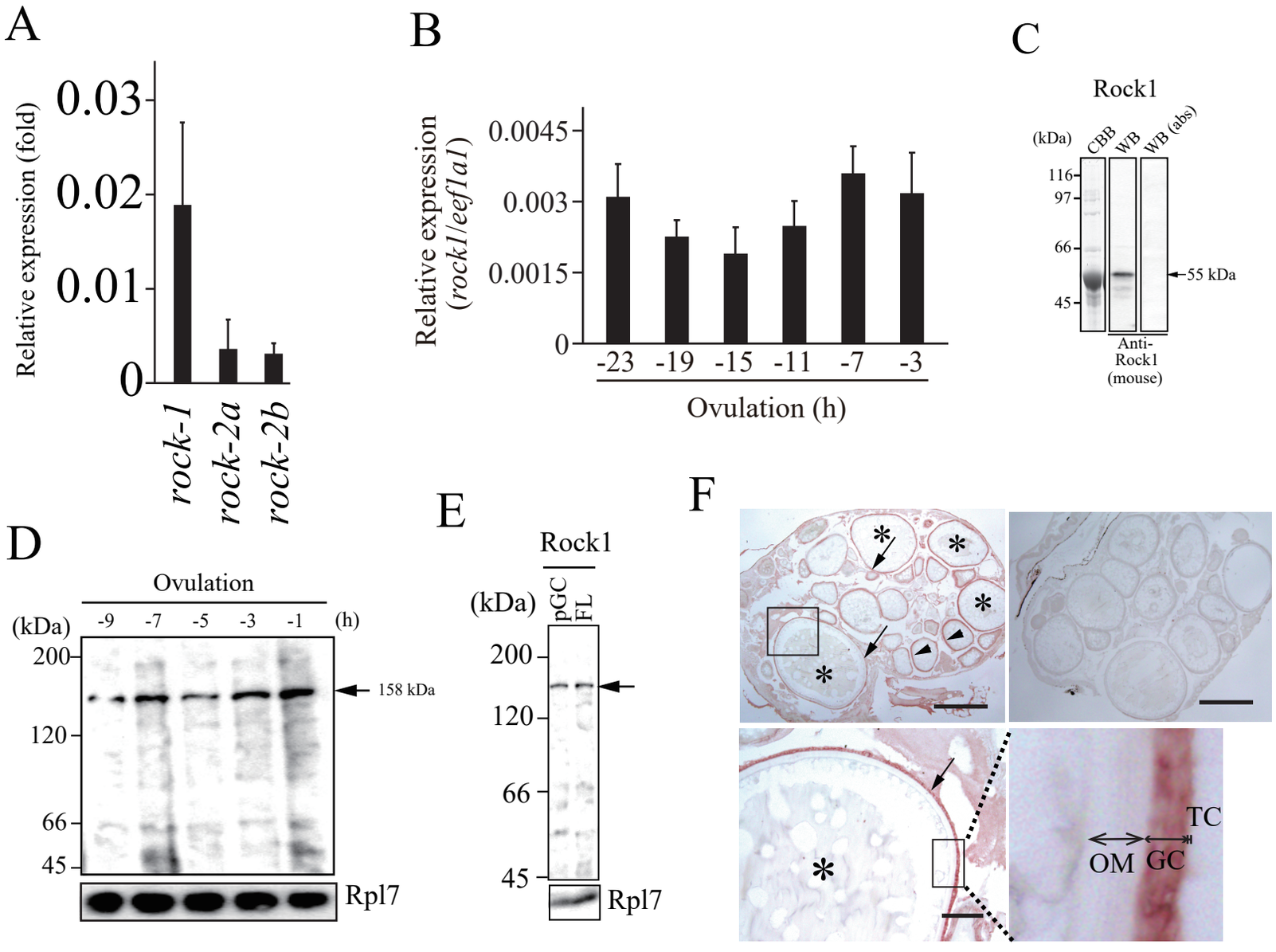
A
Relative expression (fold)
0.03
0.02
0.01
0
rock-1
rock-2a
rock-2b
B
Relative expression
(rock1/eef1a1)
0.0045
0.003
0.0015
0
-23 -19 -15 -11 -7 -3
Ovulation (h)
C
Rock1
(kDa)
CBB
WB
WB (abs)
116
97
66
45
55 kDa
Anti-
Rock1
(mouse)
D
Ovulation
(kDa)
-9 -7 -5 -3 -1 (h)
200
120
66
45
158 kDa
Rpl7
E
Rock1
(kDa)
pGC
FL
200
120
66
45
Rpl7
F
OM
GC
TC

Fig. 6

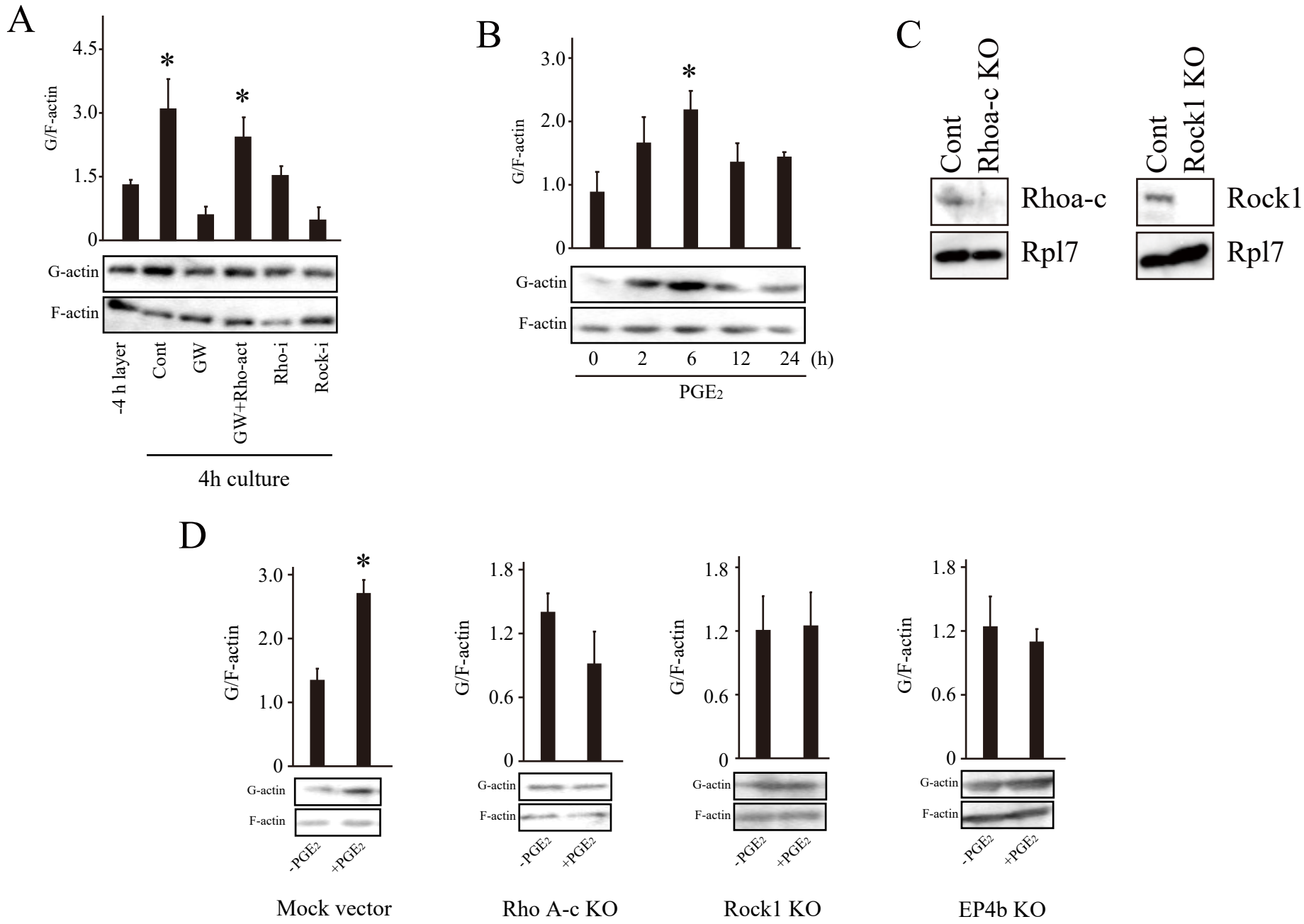
A
G/F-actin
4.5
3.0
1.5
0
*
*
G-actin
F-actin
-4 h layer
Cont
GW
GW+Rho-act
Rho-i
Rock-i
4h culture
B
G/F-actin
3.0
2.0
1.0
0
*
G-actin
F-actin
0
2
6
12
24
(h)
PGE2
C
Cont
Rhoa-c KO
Rhoa-c
Rpl7
Cont
Rock1 KO
Rock1
Rpl7
D
G/F-actin
3.0
2.0
1.0
0
*
G-actin
F-actin
-PGE2
+PGE2
Mock vector
1.8
1.2
0.6
0
Rho A-c KO
Rock1 KO
EP4b KO

Supplemental Table S1. Primers used in this study.

Primer name	gene	Sequence	Accession No.
Real-time PCR			
Rho A-a ss	*rhoa-a*	5'-CAACGACTGACGCTAACAAAG-3'	XM_004086108
Rho A-a as	*rhoa-a*	5'-CCGACTATGACCAGCTTTTTC-3'	XM_004086108
Rho A-b ss	*rhoa-b*	5'-ACTGCAAGGTCACATACATA-3'	XM_023956423
Rho A-b as	*rhoa-b*	5'-CAGGGAACTGATCCTTACTG-3'	XM_023956423
Rho A-c ss	*rhoa-c*	5'-CTCAGCGAAACGCAGTTAGA-3'	XM_004070475
Rho A-c as	*rhoa-c*	5'-CCCAACAATCACCAACTTCTT-3'	XM_004070475
Rho B ss	*rhob*	5'-CTCCTAGGAAAAGGCAGGAAT-3'	XM_004083452
Rho B as	*rhob*	5'-CTCGTCCCTGCTAAACACAAT-3'	XM_004083452
Rho G ss	*rhog*	5'-ACTCATCCATCAGCATCTAG-3'	XM_004076673
Rho G as	*rhog*	5'-AGGCTCCGGTGGTGTAGGAA-3'	XM_004076673
Rho U ss	*rhou*	5'-GTTCTGGTCGGGACACAGTG-3'	XM_004067248
Rho U as	*rhou*	5'-TCCGATCTCCACTGCACAAT-3'	XM_004067248
Rock1 ss	*rock1*	5′-TCTCTGGTTGGGACTTACAG-3′	XM_004079418
Rock1 as	*rock1*	5′-GCAGACTCTCCAGATGACTT-3′	XM_004079418
Rock2a ss	*rock2a*	5′-TGGAGGACATGCTCAGAGAC-3′	XM_023951816
Rock2a as	*rock2a*	5′-CGTAGCGCCGGGTAGTCCAA-3′	XM_023951816
Rock2b ss	*rock2b*	5′-AGGCCTTCCTCAACAGATAT-3′	XM_023952796
Rock2b as	*rock2b*	5′-CCAGCTGTACTTCTCCAAAT-3′	XM_023952796
EF1a SS	*eef1a*	5′-CACCGGTCACCTGATCTACA-3′	AB013606
EF1a AS	*eef1a*	5′-GCTCAGCCTTGAGTTTGTCC-3′	AB013606
Recombinant protein			
RhoA-a pET SS	*rhoa-a*	5'-ATGGCAGCGATCAGGAAAAAG-3'	XM_004086108
RhoA-a pET AS	*rhoa-a*	5'-TTACAGTAGGACGCATCTATT-3'	XM_004086108
RhoA-c pET SS	*rhoa-c*	5'-ATGGCCGCACTCAGAAAGAAG-3'	XM_004070475
RhoA-c pET AS	*rhoa-c*	5'-TCACAGTAGCTGGCAGCCCCC-3'	XM_004070475
Rock1 pET SS	*rock1*	5'-ATGTCCTCCGAGATAAACATG-3'	LC726226
Rock1 pET AS	*rock1*	5'-TTACAGACTCTCCAGATGACTT-3'	LC726226
Cloning			
Rock1 cds-AS	*rock1*	5′-TTAGCTCAGCTTTCCCGTGTTG-3′	LC726226

Table S1. (continued)

Primer name	gene	Sequence	Accession No.
Crsper-Cas9			
EP4b sgRNA-SS	*ptger4b*	5′-TAGGGAATGTCATCGCCATCG-3′	AB563504
EP4b sgRNA-AS	*ptger4b*	5′-AAACCGATGGCGATGACATTC-3′	AB563504
Rhoa-c sgRNA-SS	*rhoa-c*	5′-TAGGAACTACATTGCTGACATTG-3′	XM_004070475
Rhoa-c sgRNA-AS	*rhoa-c*	5′-AAACCAATGTCAGCAATGTAGTT-3′	XM_004070475
Rock-1 sgRNA-SS	*rock1*	5′-TAGGCTGGATGGCTTGGATGCTC-3′	LC726226
Rock-1 sgRNA-AS	*rock1*	5′-AAACGAGCATCCAAGCCATCCAG-3′	LC726226
RT-PCR			
EP4b-RT-SS	*ptger4b*	5′-CTGTGAGAAGGTCTTCCTAG-3′	AB563504
EP4b-RT-AS	*ptger4b*	5′-CCACCCCCTTACATCTGATT-3′	AB563504
Rhoa-c-RT-SS	*rhoa-c*	5’-ATGGCCGCACTCAGAAAGAAG-3’	XM_004070475
Rhoa-c-RT-AS	*rhoa-c*	5’-TCACAGTAGCTGGCAGCCCCC-3’	XM_004070475
Rock-1-RT-SS	*rock1*	5′-CTGAAGCTCAGCCTCTCTAA-3′	LC726226
Rock-1-RT-AS	*rock1*	5′-TGTCACCGTCAGATCCAACT-3′	LC726226
b-actin-RT-SS	*actb*	5′-CAGACACGTATTTGCCTCTG-3′	D89627
b-actin-RT-AS	*actb*	5′-CAAGTCGGAACACATGTGCA-3′	D89627